Experimental Demonstration of UAV-Based Ultra-Wideband Multi-Baseline SAR Interferometry

Victor Mustieles-Perez [a b], Julian Kanz [c], Christina Bonfert [c], Alexander Grathwohl [c], Lucas Leonardo Lamberti [a], Sumin Kim [a], Gerhard Krieger [a b], Michelangelo Villano [a]
[a] Microwaves and Radar Institute, German Aerospace Center (DLR), Germany
[b] Institute of Microwaves and Photonics, Friedrich-Alexander-Universität (FAU), Germany
[c] Institute of Microwave Engineering, Ulm University, Germany

Abstract

Unmanned aerial vehicle (UAV)-based synthetic aperture radar (SAR) interferometry (InSAR) allows for generating digital elevation models (DEMs) with unprecedented height accuracy and resolution over local areas thanks to the use of large baselines and large fractional bandwidths. A detailed DEM performance analysis unveils that under these conditions height accuracies in the order of a decimeter are feasible at spatial resolutions below 0.5 m and simulations also show that radargrammetry is accurate enough to support a pixel-wise absolute phase unwrapping. Based on these theoretical analyses, an experimental demonstration of multi-baseline InSAR is performed. The first experimental results show that the predicted height accuracies with InSAR and radargrammetry can be reached under favorable acquisition geometries and that a more refined InSAR processing is needed to deal with the nonlinearity of the trajectories and the time-variant baselines. The results will pave the way to local height measurements with unprecedented accuracy and resolution.

1 Introduction

Across-track synthetic aperture radar (SAR) interferometry (InSAR) is a technique that combines two coherent SAR images of the same scene acquired from slightly different positions separated by a geometric baseline to extract the phase difference and form a digital elevation model (DEM) of the imaged terrain [1]. The two SAR images can be acquired at different times with the radar platforms working in monostatic mode (repeat-pass interferometry) or simultaneously using two different platforms with a single transmitter (single-pass interferometry). While single-pass interferometry is to be preferred to avoid the compromising effects from undesired scene changes that may occur over short periods of time, this requires also a highly accurate synchronization between the radars on the distinct platforms [2].

In InSAR, the achievable accuracy increases with the length of the baseline, but its maximum length is limited by baseline decorrelation, which in turn depends on the bandwidth of the system. ITU regulations and other technical constraints typically pose a strong limit on the bandwidth for space- and airborne radar systems. TanDEM-X, for example, only uses a fractional bandwidth in the order of one percent in its nominal acquisition mode. In contrast, InSAR acquisitions with larger geometric baselines could provide DEMs with improved height accuracy and resolution due to a smaller scaling factor between the interferometric phase and the terrain topography. However, DEMs formed from large-baseline interferograms are also more susceptible to height ambiguities, which can be resolved in wideband systems by means of radargrammetry and/or joint processing of data acquired using more baselines [3].

Compared to air- and spaceborne systems, the use of unmanned aerial vehicles (UAVs) or drones offers some unique advantages in view of InSAR applications over local areas. Examples are reduced cost, versatile deployment, unconstrained formation flying, and less constrained bandwidths which enable larger baseline-to-height ratios and, therefore, DEMs with significantly improved accuracies and spatial resolutions [4]. These features make drones ideal for accurately studying local dynamic processes, such as small-scale topographic changes or ice melting through time series of DEMs. Nevertheless, the use of very large fractional bandwidths and baselines in InSAR has still to be experimentally addressed. Furthermore, performing InSAR with drones still represents a challenge due to the worse relative motion stability of the drones compared to conventional space- or airborne systems [5].

This paper describes the design and first results of an experimental demonstration of wide-fractional-bandwidth repeat-pass InSAR with UAVs employing multiple geometric baselines to corroborate the conclusions obtained from the theoretical analyses and simulations.

2 DEM performance analysis and experiment planning

2.1 Flights plan

A detailed analysis on the expected DEM performance has been conducted for each of the measured InSAR configurations. In the experiment, drone flying heights of 10 m, 20 m, and 30 m and linear trajectories are used to form baselines up to 30% of the critical baseline, $B_{\perp,crit}$. The conventional expression for the critical baseline is no longer valid for systems with a wide-fractional bandwidth in range. Therefore, considering the geometry in **Figure 1**, the following formulation for the critical baseline has been derived in [6]:

$$B_{\perp,crit} = \frac{|\boldsymbol{r_1}|}{\tan(\theta_1-\beta)+\frac{1}{\tan\left(\theta_1\frac{m\cdot B_F}{1+B_F/2}\right)}} \quad (1)$$

where $m = 1$ for repeat-pass and $m = 2$ for single-pass interferometry, B_F is the fractional bandwidth, β is the angle between the platforms with respect to the horizontal plane, and θ_1 and $\boldsymbol{r_1}$ are the incidence angle and the range vector from the master platform to the target, respectively. The flying accuracy of the drone is in the order of one meter in the horizontal dimension, which causes considerable uncertainty in the track which is flown by the drone and, therefore, in the baselines and the heights of ambiguity that are obtained, as illustrated in **Figure 2** for a flying height of 30 m. For this reason, the first InSAR measurements were performed with many linear tracks to ensure that a reasonable variety of baselines is obtained.

2.2 Estimated performance

The height accuracy of the final DEM depends on the interferometric coherence between the two SAR images, which can be estimated as the product of various contributions [7]:

$$\gamma_{Tot} = \gamma_{SNR} \cdot \gamma_{Amb} \cdot \gamma_{Rg} \cdot \gamma_{Vol} \cdot \gamma_{Temp} \quad (2)$$

where the different contributions correspond to limited signal-to-noise ratio (SNR) γ_{SNR}, presence of ambiguities γ_{Amb}, baseline decorrelation γ_{Rg}, volume decorrelation γ_{Vol}, and temporal decorrelation γ_{Temp}, respectively. The radar system is a frequency-modulated continuous-wave radar with the system parameters detailed in **Table 1** [8]. Although both frequency bands have been acquired in the experiment, the results included in this paper correspond to the frequency band 1. To compute the γ_{SNR}, the sigma nought model for soil and rock, VV, L-band is assumed [9].

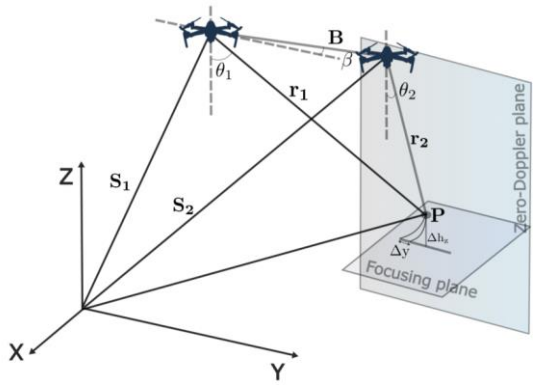

Figure 1 Geometry of an across-track InSAR acquisition, where the SAR images are focused to a common plane.

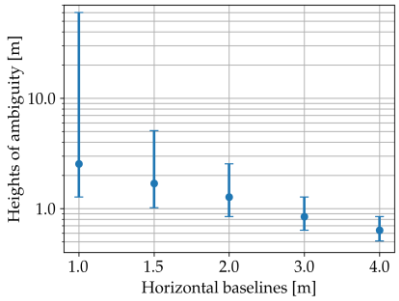

Figure 2 Predicted uncertainty in the heights of ambiguity considering the flying accuracy of the UAV and flying height of 30 m.

Table 1 Parameters of the UAV and the radar systems.

Parameter	Value	Parameter	Value
Frequency band 1	1 – 4 GHz	Tx power band 1	15 dBm
Frequency band 2	6 – 9 GHz	Tx power band 2	10 dBm
UAV speed	2 m/s	Duty cycle	0.8
Noise figure	6 dB	Antenna gain	6 dBi
Additional losses	3 dB	Antenna mounting	45˚
Pulse repetition frequency (PRF)	300 Hz	Beamwidth in azimuth	50˚
Signal quantization	12 bits	Beamwidth in elevation	60˚

The main contribution to volume decorrelation is ground penetration due to the absence of vegetation other than very short grass in the test field. It is computed using the model proposed by Hallikainen, et al. for a mid-moisturized soil and for the worst-case scenario, i.e., the lower frequency of the band [10]. The baseline decorrelation γ_{Rg} is modelled according to our previous work [6]. The range and azimuth ambiguities are negligible due to the low flying altitude and the low speed, respectively. Instead, right-left ambiguities need to be considered in γ_{Amb} due to the wide antenna beamwidth, which resulted in signal echoes in the order of -12 dB with respect to the main signal considering uniform backscattering properties. Therefore, the presence of strong targets on the contrary side may severely affect the measurements. The geometric and volume decorrelations are the most important decorrelation sources, in contrast to spaceborne systems, where the finite SNR is the limiting factor. **Figure 3** shows the predicted coherence (left) and 90th percentile of the height errors (right) for the frequency band 1, a flying altitude of 30 m above ground level and several horizontal baselines. The predicted height accuracies of the DEMs are in the decimeter range for an independent post-spacing of 0.35 m × 0.35 m. Although this is a first experiment and hence a maximum flying height of 30 m is used, the instantaneous coverage can be notably increased while keeping a great height accuracy if the transmit power is sufficient, considering the maximum height of 120 m allowed for drones.

Additional errors due to localization uncertainty need to be considered as well. The accuracy of the positioning measurements used in the SAR and InSAR processing is in the order of 10 mm and 15 mm in the horizontal and vertical dimensions, respectively, due to the use of real-time kinematic (RTK) – global positioning system (GPS). The positioning data are further enhanced by data from an inertial measurement unit (IMU) leading to sub-centimeter positioning accuracy [11]. Therefore, the DEM may have systematic displacement or tilt smaller than 2 cm and 2 cm/m, respectively, and height errors lower than 10 cm, which are reduced to less than 3 cm for large baselines [6]. Furthermore, if an additional 10% margin in the interferometric phase errors is considered to account for a possible underestimation of the interferometric coherence, additional height errors may be around 2 cm.

2.3 Phase unwrapping considerations

Phase unwrapping is challenging for large baselines because the height of ambiguity is small, leading to phase unwrapping errors within the generation of the DEM. Due to the system large fractional bandwidth, radargrammetry can

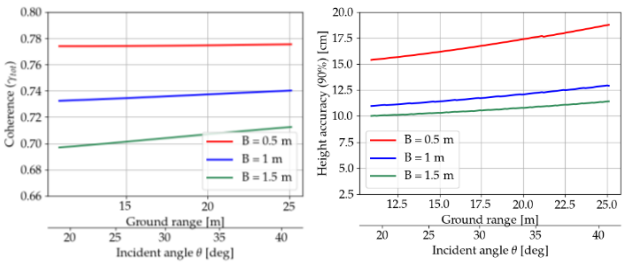

Figure 3 Predicted interferometric coherence (left) and height accuracy (90%) of the DEM for an independent post-spacing of 0.35 m × 0.35 m and a platform altitude of 30 m (right).

provide an absolute DEM with a height accuracy comparable to InSAR and smaller than the interferometric height of ambiguity. Simulations show that residual phase unwrapping errors after correction by comparison of the DEMs from InSAR and radargrammetry are smaller than 5% in the case of $B_F > 0.5$ and $\gamma_{Tot} > 0.5$. Although the employed test site does not have enough topographic height variations to produce height ambiguities, an absolute DEM is also generated using radargrammetry to verify the predicted height accuracy.

3 Experimental demonstration

The repeat-pass InSAR experiment was performed in June, 2023 using a drone-borne radar system consisting of the hexacopter DJI Matrice 600 Pro with a radar system onboard, which is shown in the top part of **Figure 4**. The parameters of the radar system are listed in **Table 1** [8]. The measurement set-up is shown in the bottom part of **Figure 4**, and consists of an area of approximately 25 m × 30 m, mostly flat with some small topographic undulations. Several trihedral corner reflectors were placed along the measured area to serve as known references. The position of the corner reflectors was measured with cm accuracy using a differential GPS station. Furthermore, a ground truth DEM of the test site was acquired with a three-dimensional laser scanner. The absolute height and inclination of the DEM obtained from the laser scanner were calibrated using the measured positions of the corner reflectors. The left-hand side of **Figure 5** shows the scheme of the experimental acquisition with the three trajectories considered in this paper, the DEM measured with the laser scanner and the position of the corner reflectors and other georeferenced stones in the scene, which are represented as red dots. The right-hand side of **Figure 5** depicts the baselines which are formed from the trajectories shown of left-hand side of the figure.

3.1 SAR focusing

The quality of the navigation data is confirmed by comparing the measured phase of a corner reflector with the phase calculated from the navigation data using the measured position of the corner reflector. The distribution of the errors exhibits a standard deviation of 0.2 cm and a 90th percentile of 0.5 cm, which are in the expected range according to the specifications of the positioning system but for an offset that has to be corrected.

Figure 4 The drone DJI Matrice 600 Pro with the radar system onboard (top) and the test field including the drone, and some corner reflectors (bottom).

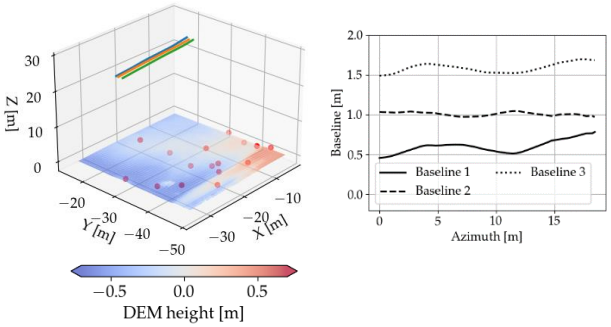

Figure 5 Scheme of the acquisitions with three trajectories represented by the blue, orange and green lines. The DEM measured with the laser scanner is also shown, and the red dots indicate the measured position of the corner reflectors and other georeferenced stones (left). Baselines formed with the three trajectories showed (right).

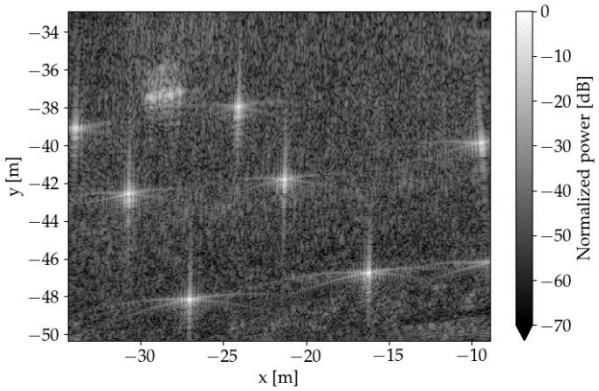

Figure 6 Focused SAR data using of an acquisition in frequency band 1 and a platform height of 30 m.

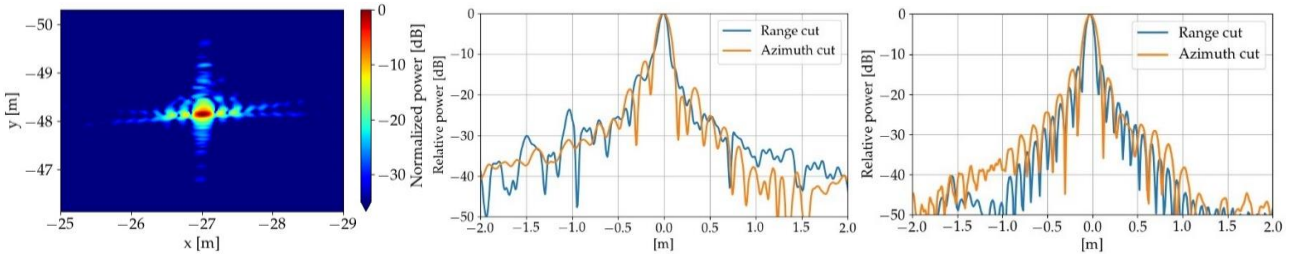

Figure 7 Measured impulse response of a trihedral corner reflector (left). For the position of the corner reflector, see **Figure 6**. Cuts in range and azimuth of the measured response (center). Simulated range and azimuth cuts of the same corner reflector simulated using the trajectory measured from the experiment (right).

The acquired SAR data are focused using back-projection. This algorithm is chosen as it can deal with the accurate localization information given by the GPS-RTK system along the non-linear tracks flown by the drone. The image is focused to a plane which is close to the ground of the imaged scene, but does not correspond to the real topography. In other cases, the SAR data can be focused as well to an a priori known coarser DEM. The SAR image is sharply focused as shown in **Figure 6**. The coordinates x and y refer to the east and north Cartesian coordinates, with the origin located in the position of the RTK station. The drone acquisition trajectory is a quasi linear trajectory approximately along the x dimension. The response to one of the corner reflectors is shown in **Figure 7** (left), and the cuts in range and azimuth are shown in **Figure 7** (center). The response of an ideal point target located at the position of the same corner reflector has also been simulated using the imaging trajectory measured in the experiment. The range and azimuth cuts of the simulated response of the point target are shown in **Figure 7** (right). The measured range and azimuth 3 dB resolutions are 6 cm and 8 cm, respectively, and agree with the expected values. The peak-to-sidelobe ratio (PSLR) in the simulated response is -14 dB, which is slightly better than the -13 dB expected for a rectangular window due to the weighting of the antenna pattern. The PSLR is 1.5 dB worse in the real data.

3.2 InSAR processing and performance

The pair of SAR images whose acquisition geometry corresponds to baseline 1 in **Figure 5** is combined to form an interferogram. As the SAR images are not focused to the exact topographic grid, coregistration is needed before forming the interferogram. The shifts that are to be applied to the slave SAR image are calculated through patch-wise coherent crosscorrelation. The wavenumber of the pixels of the SAR images depends on their position within the image [12]. Therefore, to improve the performance of the crosscorrelation, the patches are brought to baseband prior to the crosscorrelation. The shifts that are produced by patches with a low correlation coefficient are discarded, as well as the shifts that are larger than a certain threshold, which is set as the standard deviation of the surrounding shifts. The gaps are filled by an interpolation with the average of the surrounding shifts. The shifts in each of the horizontal coordinates are shown in **Figure 8** and agree with the expected values according to the geometry. The estimated coherence of the interferometric pair after coregistration is depicted in **Figure 9**. The pixels corresponding

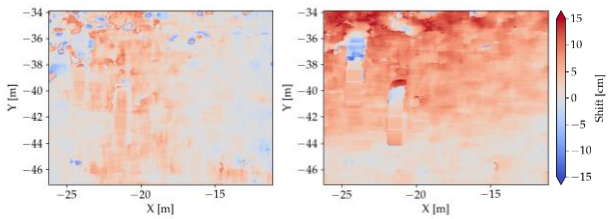

Figure 8 Map of the shifts obtained in the coregistration stage in the X (left) and Y (right) dimensions.

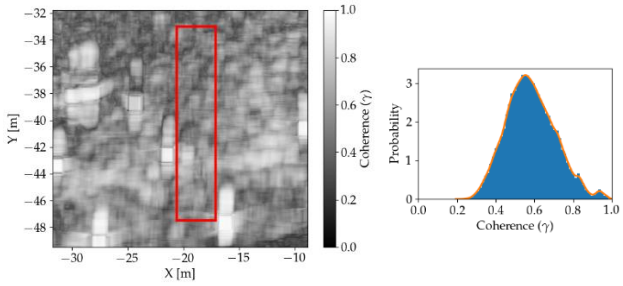

Figure 9 Estimated interferometric coherence and histogram of the coherence. The red rectangle delimits the area considered in the DEM analysis.

to a coherence close to 1 in the histogram correspond to the corner reflectors. The coherence is around 15 % lower than expected, the possible error sources include ground penetration or the time-variant baselines. The red rectangle delimits the area where the DEM performance is analyzed, as it is located in the middle of the image and less affected by the response of the corner reflectors. The formed interferogram is multi-looked using a boxcar window, resulting in an effective multilooking of 7 × 7. Having focused the SAR images in a common plane with the backprojection algorithm, the interferometric phase is related to the distance between the height of the focusing plane Δh_{foc} and the actual topographic plane. The height of ambiguity is given by:

$$h_{2\pi} = \frac{\lambda}{m \cdot (\cos\theta_1 - \cos\theta_2)}. \quad (3)$$

Figure 10 shows the DEMs obtained from the three-dimensional laser scanner (left) and InSAR (right). The baseline in the selected area is almost constant around 0.5 m, as represented by the baseline 1 in the right hand-side of **Figure 5**, which yields a height of ambiguity of around 3 m. **Figure 11** depicts the errors between the DEMs from the laser scanner and InSAR (note the different color scales). The absolute height of the DEM had an offset with respect

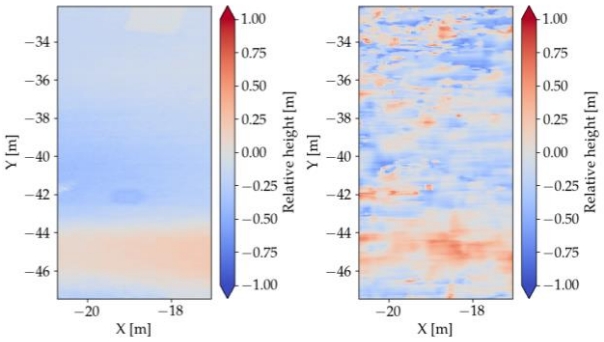

Figure 10 DEMs formed from the laser scanner measurement (left) and InSAR (right).

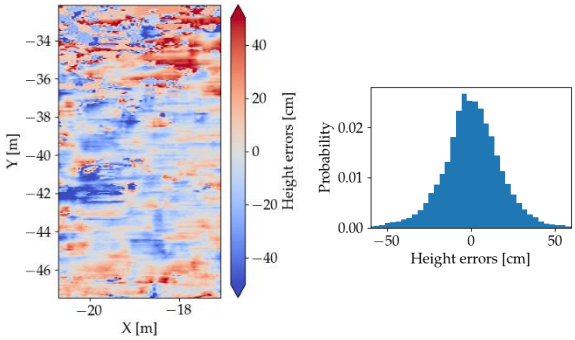

Figure 11 Height errors in the DEM obtained from InSAR, when comparing it with the DEM from the laser scanner.

to the one measured by the laser scanner, which was corrected. The standard deviation and 90th percentile of the height errors are 25 cm and 43 cm, respectively, which is around 10 cm worse than expected. The error sources that cause these height differences may be related to the time-variant baselines, effects due to the large fractional bandwidth, processing artifacts, and/or varying penetration into the ground, and will be analyzed in detail in the future.

3.3 Radargrammetric processing and performance

A further DEM can be also formed using radargrammetry, i.e., exploiting the shifts obtained in the coregistration stage. The height accuracy that can be obtained depends on the accuracy of the shift estimation, which depends on the range resolution of the radar, the baseline and the terrain features. Considering the system geometry in **Figure 1**, the topographic height difference with respect to the focusing plane Δh_z can be geometrically derived solving the following system of equations [13]:

$$|\boldsymbol{r_2}|^2 = |\boldsymbol{r_1}|^2 + |\boldsymbol{B}|^2 + 2 \cdot |\boldsymbol{r_1}| \cdot |\boldsymbol{B}| \cdot \sin(\theta_1 - \beta), \quad (4)$$

$$\Delta h_z = |\boldsymbol{r_1}| \cdot \cos\theta_1 - (H_1 - h_{foc}). \quad (5)$$

where $\boldsymbol{r_2}$ is the range vector from the slave platform to the target, $\boldsymbol{B}$ is the vector of the baseline between the platforms, H_1 is the height of the master platform and h_{foc} is the height of the focusing plane. **Figure 12** shows the DEMs obtained using radargrammetry for the baselines 1 (left) and 2 (right). The achieved standard deviations of the

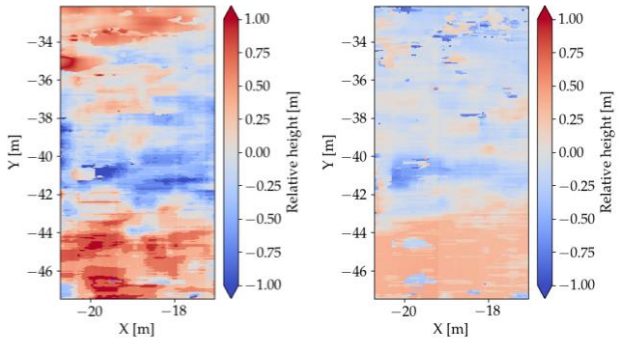

Figure 12 DEMs formed from the estimated shifts using radargrammetry with the baselines 1 (left) and 2 (right) of **Figure 5**.

errors are 0.41 m and 0.20 m, respectively, which reasonably match the expected accuracies of 0.37 m and 0.18 m. Therefore, the accuracy of the DEM from radargrammetry is sufficient to support phase unwrapping. Considering the acquisition with baseline 1, the absolute value of the height difference between the DEM from radargrammetry and the DEM from InSAR is larger than half the height of ambiguity in only 0.4% of the cases, which agrees with a value of less than 1% obtained in the simulations. Hence the phase unwrapping can be effectively performed by pixelwise comparison between the absolute DEM from radargrammetry and the DEM obtained from InSAR. In cases where the bandwidth is smaller, the accuracy of the DEM from radargrammetry can be improved to achieve the required phase unwrapping performance by using an acquisition with a second larger baseline, as shown in **Figure 12** on the right.

4 Conclusions and outlook

A measurement campaign involving a large number of acquisitions in different interferometric configurations has been performed in June, 2023 to validate the theoretical performance of UAV-based multi-baseline InSAR. The first results of the experiment show that accuracies in the order of a decimeter can be reached with both InSAR and radargrammetry, but effects such as the non-constant baseline and the ground penetration throughout the wide bandwidth have to be considered as well. Therefore, the next steps include both analyzing in detail the different error sources and considering the joint processing of interferograms generated from different baselines and frequency bands together.

While our first demonstration campaign considered only platform heights up to 30 m above ground level, current drone regulations allow for flying altitudes up to 120 m. This will allow reasonable coverages, e.g., 1 km^2 in 30 minutes will be feasible with a single pair of drones, which can be extended by using a drone swarm. Our results will not only open the door to a new generation of DEMs and height change maps for several local-scale applications, but they will also serve for the preparation of future wide-band, multi-frequency and/or multi-platform spaceborne SAR missions.

5 Acknowledgements

This work was partially funded by the Deutsche Forschungsgemeinschaft (DFG, German Research Foundation) GRK 2680 – Project-ID 437847244.
Co-funded by the European Union (ERC, DRITUCS, 101076275). Views and opinions expressed are however those of the authors only and do not necessarily reflect those of the European Union or the European Research Council Executive Agency. Neither the European Union nor the granting authority can be held responsible for them.

6 Literature

[1] P. A. Rosen et al., “Synthetic aperture radar interferometry,” Proceedings of the IEEE, vol. 88, Art. no. 3, Mar. 2000.

[2] R. Bamler and P. Hartl, “Synthetic aperture radar interferometry,” Inverse Problems, vol. 14, Art. no. 4, Aug. 1998.

[3] G. Krieger and A. Moreira, “Multistatic SAR satellite formations: potentials and challenges,” in Proceedings. 2005 IEEE International Geoscience and Remote Sensing Symposium, 2005. IGARSS ’05., 2005, vol. 4, pp. 2680–2684.

[4] A. Grathwohl et al., "Taking a Look Beneath the Surface: Multicopter UAV-Based Ground-Penetrating Imaging Radars," in IEEE Microwave Magazine, vol. 23, no. 10, pp. 32-46, Oct. 2022.

[5] S. Jeon, et al., “UAV-Borne Bistatic SAR and InSAR Experiments in Support of STV and SDC Target Observables,” IGARSS 2023, Pasadena, CA, USA, 16-21 July 2023.

[6] V. Mustieles-Perez, S. Kim, C. Bonfert, G. Krieger, and M. Villano, “Towards UAV-Based Ultra-Wideband Multi-Baseline SAR Interferometry,” EuRAD 2023, Berlin, Germany, 20-22 September 2023

[7] G. Krieger et al., “TanDEM-X: A Satellite Formation for High-Resolution SAR Interferometry,” IEEE Transactions on Geoscience and Remote Sensing, vol. 45, Art. no. 11, Nov. 2007.

[8] R. Burr et al., “UAV-Borne FMCW InSAR for Focusing Buried Objects,” in IEEE Geoscience and Remote Sensing Letters, vol. 19, pp. 1–5, 2022.

[9] F. Ulaby, M. Craig Dobson, and J. L. Alvarez Perez. Handbook of Radar Scattering Statistics for Terrain. Norwood, MA: Artech House, 1989

[10] M. T. Hallikainen, F. T. Ulaby, M. C. Dobson, M. A. El-rayes and L. -k. Wu, "Microwave Dielectric Behavior of Wet Soil-Part 1: Empirical Models and Experimental Observations," in IEEE Transactions on Geoscience and Remote Sensing, vol. GE-23, no. 1, pp. 25-34, Jan. 1985.

[11] R. Bahnemann et al., “Under the sand: Navigation and localization of a micro aerial vehicle for landmine detection with ground-penetrating synthetic aperture radar,” Field Robotics, 2021.

[12] A. W. Doerry, E. E. Bishop, and J. A. Miller, “Basics of backprojection algorithm for processing synthetic aperture radar images,” Sandia Rep. SAND2016-1682, p. 58, 2016.

[13] C. Rossi, “Uncertainty assessment of single-pass TanDEM-X DEMs in selected applications,” Ph.D. dissertation, Institute of Photogrammetry and Cartography, Tech. Univ. of Munich, Munich, Germany, 2016.